

KINEMATIC RECONNECTION AT A MAGNETIC NULL POINT: SPINE-ALIGNED CURRENT

D.I. PONTIN^{a,*}, G. HORNIG^b and E.R. PRIEST^a

^a*School of Mathematics and Statistics, University of St. Andrews, St. Andrews, Fife, KY16 9SS, Scotland, UK*

^b*Theoretische Physik IV, Ruhr-Universiteit, D-44780, Bochum, Germany*

(Received 6 February 2004; In final form 17 May 2004)

Magnetic reconnection at a three-dimensional null point is the natural extension of the familiar two-dimensional X-point reconnection. A model is set up here for reconnection at a spiral null point, by solving the kinematic, steady, resistive magnetohydrodynamic equations in its vicinity. A steady magnetic field is assumed, as well as the existence of a localised diffusion region surrounding the null point. Outside the diffusion region the plasma and magnetic field move ideally. Particular attention is focussed on the way that the magnetic flux changes its connections as a result of the reconnection. The resultant plasma flows are found to be rotational in nature, as is the change in connections of the magnetic field lines.

Keywords: Magnetic reconnection; Magnetohydrodynamics; Magnetic flux; Magnetic null points

1 INTRODUCTION

Magnetic reconnection is a fundamental process in many areas of plasma physics, whereby the magnetic field, \mathbf{B} , becomes restructured. When null points are present the global topology of the field changes. Our ideas on how this restructuring occurs come mostly from the well-studied case of reconnection in two dimensions. In two dimensions, reconnection occurs at hyperbolic null points of the magnetic field (see, e.g. Priest and Forbes, 2000, for a review), commonly known as X-points (see Fig. 1). A plasma flow transports magnetic flux towards the X-point, where the reconnection takes place, and the flow then transports the reconnected magnetic flux away from the X-point. In terms of magnetic field lines, the process of reconnection involves a pair of field lines being brought in from two quadrants on opposite sides of the null. At the X-point each of these field lines breaks, when they lie along the separatrices of the field. They are then rejoined and move out in the other two quadrants of \mathbf{B} . The result is that the field line footpoints are pair-wise differently connected when they leave the reconnection region.

*Corresponding author. E-mail: davidp@mcs.st-and.ac.uk

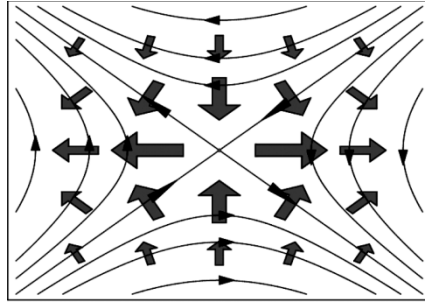


FIGURE 1 Two-dimensional reconnection at an X -point. The thin lines are magnetic field lines and the bold arrows indicate the direction of the plasma flow.

Magnetic reconnection is a fundamentally non-ideal process; in an ideal plasma, magnetic field lines maintain their identity for all time, and are said to be ‘frozen-into’ the plasma. The non-idealness may be the result, for example, of a non-zero resistivity, η , in which case, assuming no other non-ideal effects are important, the process satisfies Ohm’s law in the form

$$\mathbf{E} + \mathbf{v} \times \mathbf{B} = \eta \mathbf{J}. \quad (1)$$

In order to investigate the evolution of magnetic flux it is useful to define a flux transporting velocity \mathbf{w} (Hornig and Schindler, 1996; Hornig and Priest, 2003) which satisfies

$$\mathbf{E} + \mathbf{w} \times \mathbf{B} = \mathbf{0}, \quad (2)$$

which is possible in two dimensions since the electric field, \mathbf{E} , is always perpendicular to \mathbf{B} . Note that for reconnection to take place, the flux transporting velocity \mathbf{w} must become singular at the null point, which is a signature of the breaking of the field lines (Hornig, 2001) and the subsequent discontinuity in the mapping of their endpoints. By comparison with an ideal Ohm’s law, we can consider \mathbf{w} to be a flow within which the magnetic flux is frozen. The component of \mathbf{w} perpendicular to \mathbf{B} can be found from

$$\mathbf{w}_{\perp} = \mathbf{E} \times \mathbf{B} / B^2. \quad (3)$$

If we assume that the non-ideal term on the right-hand side of Eq. (1) is localised within a finite region, D , about the null point, then outside D , \mathbf{w} coincides with the plasma velocity perpendicular to \mathbf{B} , \mathbf{v}_{\perp} .

The situation in three dimensions is much more complicated. In general, for reconnection in three dimensions, $\mathbf{E} \cdot \mathbf{B}$ (or $\mathbf{J} \cdot \mathbf{B}$) is non-zero within a finite region D , and hence in general no unique flux-conserving velocity exists, or in other words there is no unique field line velocity for field lines which thread D (for a proof, see Hornig and Schindler, 1996; Priest *et al.*, 2003). Nonetheless, it is still possible to study the evolution of magnetic flux and field lines under certain circumstances. Consider the case of a resistive non-ideal term $\eta \mathbf{J}$, which is localised within some diffusion region, D . We consider a finite region D as the generic situation for astrophysical plasmas since

these plasmas have extremely high magnetic Reynolds numbers, and dissipation is enhanced in well localised regions, for example, when micro instabilities form in a thin current sheet.

If no closed magnetic field lines exist within D , then we can still follow the motion of individual field lines from each end, since we know that in the ideal region on either side of D they must remain attached to the same plasma elements for all time. Suppose the surface of D is split into two parts, through one of which magnetic flux enters D , and through the other of which it leaves. Since each field line is anchored twice in the ideal environment, once on either side of the non-ideal region, one can follow the motion of the field lines by tracing them through space from either of these two sets of footpoints. By reference to the ideal environment then, it is possible to define a velocity with which the field lines passing *into* D move, say \mathbf{w}_{in} , and another velocity \mathbf{w}_{out} at which the field lines passing *out of* D move. In the stationary case, these two velocities can be calculated throughout space by mapping the electric potential from each set of footpoints along the field lines. This leads us to the mathematical expressions given in Eqs. (26) and (27). These two (pseudo-)field line velocities must each be identical to \mathbf{v}_\perp on the relevant section of the surface of D , but in contrast to the two-dimensional case, they are not identical to each other inside D , nor are they identical to \mathbf{v}_\perp on their continuations through D . This is a manifestation of the non-existence of a unique field line velocity, \mathbf{w} , as stated above. The result is that, following field lines with \mathbf{w}_{in} and \mathbf{w}_{out} , respectively, the field lines seem to split as soon as they are transported into the diffusion region, and inside D they continually change their connections.

Reconnection can occur in three dimensions either at a null point or in the absence of a null point (Schindler *et al.*, 1988; Lau and Finn, 1990; Priest and Forbes, 2000). The nature of the field line splitting, and subsequent restructuring of the magnetic flux, for reconnection in a simple magnetic structure with no null point has been discussed in general by Priest *et al.* (2003), and in more detail by Horing and Priest (2003). Here we study instead the kinematic problem at a three-dimensional null point. We find that the induction equation implies that such reconnection is profoundly different from two-dimensional X-point reconnection. The implications for further study are addressed in the conclusion.

In Section 2, we describe the structure of three-dimensional null points as well as describing ideal field line behaviour in their vicinity. In Section 3, the equations solved in our model are given, as well as the assumptions made, and we detail our method of solution. The elementary solution is given in Section 4, before we describe the result of adding a physically relevant ideal flow in Section 5. The existence of perfectly reconnecting flux tubes is discussed in Section 6, where the effect of adding a simple time-dependence to the model is described. We give our conclusions in Section 7.

2 STRUCTURE OF 3D NULL POINTS AND IDEAL BEHAVIOUR

The nature of reconnection at a three-dimensional null point is of particular interest since it is the three-dimensional generalisation of an X-point. Three-dimensional null points are also of crucial importance in the topology and interaction of complex fields on the Sun. They are found in abundance in the solar corona (see e.g. Brown and Priest, 2001; Longcope *et al.*, 2003), where their associated separatrices

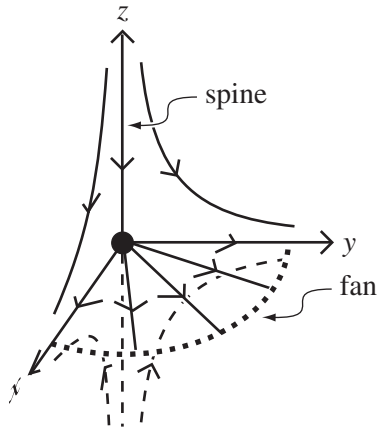


FIGURE 2 Basic structure of a three-dimensional null point.

and separators are thought to be likely candidates for sites of coronal heating (Longcope, 1996; Antiochos *et al.*, 2002; Priest *et al.*, 2002). There is also evidence that null point reconnection may act as a trigger for at least some solar flares (Fletcher *et al.*, 2001). The local structure of the magnetic field around a three-dimensional null point is shown in Fig. 2. The *skeleton* of the null point is made up of a pair of field lines directed into (or out of) the null from opposite directions, known as the *spine*, and a family of field lines which are directed out of (or into) the null lying in a surface, known as the *fan* plane (Priest and Titov, 1996). A general mathematical formalism is given by Parnell *et al.* (1996), who classify nulls depending, amongst other things, on the size of the current, \mathbf{J} , and its direction with respect to the spine axis and fan plane. If the current is zero then the null point is known as *potential*. When the current is directed only parallel to the spine ($\mathbf{J} = \mathbf{J}_{\parallel}$), the fan and spine are perpendicular, and the field lines in the fan form a spiral structure (Parnell *et al.*, 1996). When the current is directed only perpendicular to the spine ($\mathbf{J} = \mathbf{J}_{\perp}$), the spine and fan are no longer perpendicular. In general, when the current has components in both directions, both of these effects are present, as well as further characteristics, depending on the relative magnitudes of \mathbf{J}_{\parallel} and \mathbf{J}_{\perp} .

The kinematics of steady reconnection at a three-dimensional null point have been studied previously by Priest and Titov (1996). They start off by discussing the ideal behaviour in the vicinity of the simple potential magnetic null given by

$$\mathbf{B} = (x, y, -2z). \quad (4)$$

The reconnection is classified as one of two types near an isolated null point, termed *spine reconnection* and *fan reconnection*. Reconnection associated with a separator, a special field line which joins two null points, is also discussed. Due to the fact that the configuration considered is ideal, to achieve reconnection, the plasma velocity is necessarily singular at the null, and the field line mapping is discontinuous. During spine reconnection a flow is imposed across the fan ($z=0$) resulting in singularities in \mathbf{E} and \mathbf{v} at the spine ($x=y=0$). In fan reconnection, the flow is imposed across

the spine resulting in singularities in \mathbf{E} and \mathbf{v} in the fan plane. The effect of adding non-potential and diffusive terms is then considered in a preliminary manner.

We aim here to investigate the structure of reconnection when the null point is non-potential, with a current parallel to the spine, where a localised diffusion region is included in order to get a realistic model with no singularities in any physical quantities.

It is instructive to seek insight into the structure of the highly complex process of three-dimensional reconnection by considering solutions to a reduced set of the MHD equations. We follow the method of Hornig and Priest (2003) in adopting the kinematic approximation, by solving the induction equation and Maxwell's equations, though not solving the equation of motion. In a dynamical situation we would expect to start from an initial field, which then forms a current sheet (diffusion region) at which reconnection takes place. The way in which a current sheet may form by the collapse of such null points is discussed by Parnell *et al.* (1997) and Mellor *et al.* (2003) as well as by Klapper *et al.* (1996) and Bulanov and Sakai (1997). It should be noted, however, that as in two dimensions, reconnection may be initiated in many different ways (see e.g. Priest and Forbes, 2000), such as by driving from boundaries, or as a result of instabilities of many different types, as well as by null point collapse (following response to external boundary motions). Our investigation here is independent of the initiation mechanism.

3 THE MODEL

We seek a solution of the kinematic, steady, resistive MHD equations given by

$$\mathbf{E} + \mathbf{v} \times \mathbf{B} = \eta \mathbf{J}, \quad \nabla \times \mathbf{E} = \mathbf{0}, \quad (5, 6)$$

$$\nabla \cdot \mathbf{B} = \mathbf{0}, \quad \nabla \times \mathbf{B} = \mu_0 \mathbf{J}. \quad (7, 8)$$

The non-ideal term on the right-hand side of Eq. (5) is assumed to be localised, for the reasons described in Section 1.

We investigate the behaviour in the vicinity of a simple spiral null point, where \mathbf{J} lies parallel to the spine. In the future, we will go on to consider the case where \mathbf{J} is perpendicular to the spine. In general the field in the vicinity of our spiral null point can be written (Parnell *et al.*, 1996) as

$$\mathbf{B} = B_0 \left(x - \frac{1}{2} j y, y + \frac{1}{2} j x, -2z \right), \quad (9)$$

where B_0 and j are constants, such that $\mathbf{J} = (B_0 j / \mu_0) \hat{\mathbf{z}}$ (from Eq. (8)) is directed along the z -axis, which is coincident with the spine. Due to the cylindrical symmetry of the field, it simplifies matters to work in cylindrical polar coordinates (R, θ, z) , in which \mathbf{B} has the form

$$\mathbf{B} = B_0 \left(R, \frac{1}{2} j R, -2z \right). \quad (10)$$

It is crucial for the following analysis to be performed analytically that we are able to find analytical equations describing the field lines in terms of some initial starting

coordinates, \mathbf{x}_0 . For \mathbf{B} defined as in Eq. (10), this can be done by integrating

$$\frac{d\mathbf{X}(s)}{ds} = \mathbf{B}(\mathbf{X}(s)) \quad (11)$$

to find $\mathbf{X}(\mathbf{x}_0, s)$, given by Eq. (12), as

$$R = R_0 \exp(B_0 s), \quad \theta = \theta_0 + \frac{1}{2} B_0 j R s, \quad z = z_0 \exp(-2B_0 s). \quad (12)$$

Note that the parameter s does not denote the distance, dl , along a field line, which is instead given by

$$dl = |B| ds. \quad (13)$$

From Eq. (6) we can see that \mathbf{E} can be written as the gradient of some scalar, Φ say, so that Eq. (5) becomes

$$-\nabla\Phi + \mathbf{v} \times \mathbf{B} = \eta \mathbf{J}. \quad (14)$$

A solution to this equation for given \mathbf{B} may be found as follows. Firstly, since we require our non-ideal term to be localised and since \mathbf{J} is constant, we prescribe a localised resistivity, η . The component of Eq. (14) parallel to \mathbf{B} is $-(\nabla\Phi)_{\parallel} = \eta \mathbf{J}_{\parallel}$, which may be integrated along field lines to give

$$\Phi = - \int \eta \mathbf{J}_{\parallel} dl + \Phi_0 = - \int \eta \mathbf{J} \cdot \mathbf{B} ds + \Phi_0. \quad (15)$$

Thus, if we can prescribe some function $\eta = \eta(\mathbf{x}_0, s)$ in such a way that, having substituted Eq. (12) into \mathbf{B} and \mathbf{J} to find $\mathbf{B}(\mathbf{x}_0, s)$ and $\mathbf{J}(\mathbf{x}_0, s)$, Eq. (15) is integrable, then we can deduce $\Phi(\mathbf{x}_0, s)$. From here it is possible to substitute the inverse of Eq. (12) to find $\Phi(\mathbf{x})$. Then the electric field, \mathbf{E} , and the component of the plasma velocity perpendicular to \mathbf{B} , \mathbf{v}_{\perp} , can be found from

$$\mathbf{E} = -\nabla\Phi \quad (16)$$

and

$$\mathbf{v}_{\perp} = (\mathbf{E} - \eta \mathbf{J}) \times \mathbf{B} / B^2. \quad (17)$$

Prescribing a physically reasonable profile for $\eta(\mathbf{x})$ we can obtain an expression for η in terms of the field line coordinates (\mathbf{x}_0, s) with the help of the coordinate transformations (Eq. (12)). This expression can then be used for the integration (Eq. (15)). In order to have a unique coordinate transformation $\mathbf{x} \rightarrow (\mathbf{x}_0, s)$, we need to choose the initial points \mathbf{x}_0 on surfaces such that each field line passes through these surfaces exactly once. Two obvious choices which we will use in the following discussions are the planes $z = \pm 1$, or a cylindrical surface such as $R = 1$.

It is now necessary to choose $\eta(\mathbf{x})$ in such a way that the integral in Eq. (15) can be performed analytically. One analytically integrable form for $\eta(\mathbf{x})$ is a piecewise polynomial function, such as

$$\eta = \eta_0 \begin{cases} [(R/a)^2 - 1]^2 [(z/b)^2 - 1]^2 & R < a, z^2 < b^2, \\ 0, & \text{otherwise,} \end{cases} \quad (18)$$

where η_0 , a and b are constant and η_0 is the value of the resistivity, η , at the null point. This form of η gives a cylindrical diffusion region, of radius $R = a$, say, extending in the z -direction to $\pm b$. We are choosing this shape for simplicity, and aim to consider other shapes in the future. η is continuous and smooth everywhere. To proceed we need to perform the integration given by Eq. (15). In order to do this we must choose in which direction along the magnetic field lines to integrate. That is, we may choose either to set $s = 0$ on some surface of $R = R_0$ (where R_0 is a constant, $R_0 > a$) and integrate in towards the null point and thus through D , or we may integrate down and up towards the null from $z = z_0$ and $z = -z_0$, respectively (constant $z_0 > b$), setting $s = 0$ on these surfaces for each half-space. In the latter case the starting potentials (Φ_0) at $z = \pm z_0$ must be chosen such that Φ is continuous and smooth at the fan plane ($z = 0$). However, the choice between these two directions of integration is irrelevant provided we consider our model with respect to some chosen external/boundary conditions, equivalent to imposing some Φ on one boundary. The results from each case then are equivalent, and so we choose here to describe the result of setting $s = 0$ on $z = \pm z_0$, constant, and point out any significant differences for the other case when they occur.

By the method described above, $\mathbf{E}(\mathbf{x})$ can be found. However, it turns out that for the choice of η given in Eq. (18), \mathbf{E} is singular in the fan ($z = 0$). The reason is that η is not sufficiently flat near the null point, where the diverging field lines make the integration of Φ very sensitive to any variations of η . To obtain a smooth (and therefore physically acceptable) \mathbf{E} , we find that the power of the variables in Eq. (18) must be greater than 4, and so take, for simplicity,

$$\eta = \eta_0 \begin{cases} [(R/a)^6 - 1]^2 [(z/b)^6 - 1]^2 & R < a, z^2 < b^2, \\ 0 & \text{otherwise,} \end{cases} \quad (19)$$

where η_0 , a and b have the same physical meanings as before. This form for η has essentially the same structure as that given by Eq. (18).

It is now possible, via the method described at the beginning of this section, to calculate \mathbf{E} and \mathbf{v}_\perp . The analytical expressions for these are too lengthy to present here, but can be calculated using a symbolic computation program. The resulting solution, described in detail in the following section, gives, in a sense, a local rearrangement of the flux within an envelope of field lines enclosing the diffusion region, D , see Fig. 3.

The rearrangement is local in the sense that Φ only changes on field lines which pass through D (see Eq. (15)), and thus in a region of space threaded exclusively by field lines which have not passed through D , Φ is constant, and Eqs. (16) and (17) imply that \mathbf{E} and \mathbf{v}_\perp are zero.

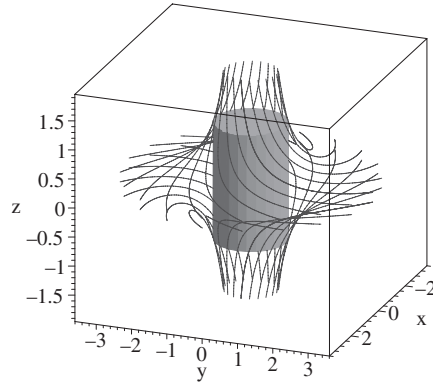


FIGURE 3 Field lines on the boundary of the envelope enclosing the diffusion region (cylinder), showing the region of influence of the local solution.

Now, for a given magnetic field, Ohm's law (Eq. (14)) may be decomposed into an ideal component (Eq. (21)) and a non-ideal component (Eq. (20)) as follows

$$-\nabla\Phi_{non-id} + \mathbf{v}_{non-id} \times \mathbf{B} = \eta\mathbf{J}, \quad (20)$$

$$-\nabla\Phi_{id} + \mathbf{v}_{id} \times \mathbf{B} = \mathbf{0}. \quad (21)$$

We have the freedom to add an ideal flow to the non-ideal solution since we do not solve the momentum balance equation here, which would otherwise determine the ideal part of the flow.

We can thus add an ideal flow to our 'local' solution by taking Φ_{id} to be our Φ_0 in Eq. (15). Note that Φ_{id} should be constant with respect to the integration in Eq. (15), i.e. $\Phi_{id} = \Phi_{id}(\mathbf{x}_0)$. The perpendicular component of the ideal flow $\mathbf{v}_{id\perp}$ may then be calculated, by taking the cross-product of Eq. (21) with \mathbf{B} , as

$$\mathbf{v}_{id\perp} = -\nabla\Phi_{id} \times \mathbf{B}/B^2. \quad (22)$$

We may thus add an ideal flow to transport magnetic flux into and out of the local envelope shown in Fig. 3, allowing us to see the global effect of the restructuring of the magnetic flux by the reconnection process. This will be discussed in Section 5, but first let us consider the elementary solution.

4 ELEMENTARY SOLUTION

4.1 Induced Flows

We examine here the nature of the solution with $\Phi_{id} = 0$, i.e. just the local behaviour of the flux envelope enclosing D with no extra ideal flow. All physical quantities are completely symmetric about $z = 0$, and we will therefore describe the results only for $z > 0$. Choosing to integrate Eq. (15) from $z = z_0$ we automatically start with Φ constant for $z > b$. Hence the electric field and plasma velocity are zero for $z > b$. The velocity for

$z < b$ is a rotation within the flux envelope. (For integration from $R = R_0$, the plasma velocity, \mathbf{v} , vanishes for $R > a$, and we have a rotation within the remainder of the flux envelope.)

For the purposes of illustration of the results, it is at this stage convenient to add a component of \mathbf{v} parallel to \mathbf{B} such that $v_z = 0$. This is achieved by defining

$$\mathbf{v} = \mathbf{v}_\perp - (v_{\perp z}/B_z)\mathbf{B}. \tag{23}$$

Our freedom to do this comes from the fact that Eq. (14) determines only the perpendicular component of \mathbf{v} , since it is the part that affects the behaviour of the magnetic flux, and so for our purposes the parallel component is arbitrary. The resulting flow pattern of \mathbf{v} in a plane of constant z is shown in Fig. 4a. The radial component, as well as by definition the z -component, of \mathbf{v} is zero, so we have purely rotational flow, and the way that this varies with radius is shown in Fig. 4b. Note that here the angular plasma velocity is strongest in a ring centred on the spine. Note also that in the $z=0$ plane the fan field lines rotate like a solid body, as does the plasma outside the diffusion region.

The source of the rotational flows can be explained as follows. We consider the case where Φ is integrated from $z = z_0$, and the argument can be easily adapted to the reverse integration. Consider the potential drop along sections of the loop illustrated in Fig. 5. $L1$ and $L3$ are radial lines in planes $z=b$ and $z < b$, respectively, while $L2$ is a field line on the surface of the envelope of flux threading D , and $L4$ lies along

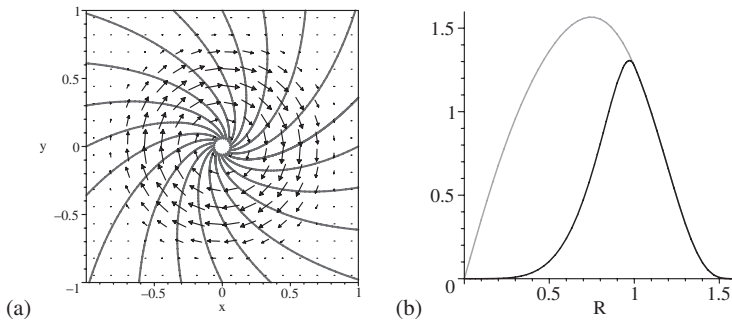


FIGURE 4 (a) Vectors of the plasma flow \mathbf{v} , along with a projection of the magnetic field lines in the plane $z = 0.4$, for the parameters $B_0 = 1, a = 1, b = 1, \eta_0 = 1, j = 2$. The corresponding radial variation of the plasma velocity v_θ (black line) and field line velocity $w_{out\theta}$ (grey).

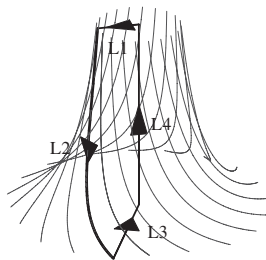


FIGURE 5 Closed loop made up of line sections. $L1$ and $L3$ are radial lines in planes $z=b$ and $0 < z < b$ respectively. $L2$ is a field line lying on the surface of the flux envelope enclosing D , and $L4$ lies along the spine ($R=0$).

the spine of the null. The potential drop around any closed loop must be zero. The potential drop along lines $L1$ and $L2$ must be zero, as $L1$ lies at $z \geq b$ and $L2$ lies on the boundary of the envelope, and so $\Phi = \Phi_0$ all along them. Thus

$$\Delta\Phi_{L3} + \Delta\Phi_{L4} = 0,$$

or

$$\Delta\Phi_{L3} = -(\Phi_{spine} - \Phi_0) \neq 0, \quad (24)$$

where Φ_{spine} is the value of Φ at the vertex of $L3$ and $L4$, which must be different from Φ_0 since \mathbf{E} is non-zero along the spine ($\mathbf{E} \cdot \mathbf{B} = \mathbf{J} \cdot \mathbf{B} \neq 0$ on spine). Since there is a potential drop along $L3$ there must also be a non-zero electric field along it. This electric field induces a plasma flow perpendicular to such a radial line, i.e. a rotational flow. This rotation has the same sense for $z > 0$ and $z < 0$, and has maximum magnitude in the $z=0$ plane. Note that this argument is completely independent of the particular profile of η within D .

4.2 Reconnection Rate

It is possible to calculate a reconnection rate for the flux in this reconnection process, although it is important to note that this has a very different physical meaning from the concept of a reconnection rate in two-dimensional reconnection. In two dimensions, flux is cut and rejoined at the null point, and the reconnection rate gives a measure of the amount of flux that undergoes this process in a given time. However, in three dimensions we need a different definition since we have a localised flux envelope within which all of the flux continually changes its connections, so during an arbitrarily short length of time every field line is reconnected (except, for symmetry reasons, the spine field line).

Considering just the flux reconnected in the half-space $z > 0$, we define, by close analogy to Hornig and Priest (2003), the reconnection rate, F , as the integral over the parallel electric field along the spine axis,

$$\begin{aligned} F &= \int_{z=0}^{\infty} (E_{\parallel})_{R=0} dl = \Phi(R=0, z=b) - \Phi(R=0, z=0) \\ &= \frac{72}{91} B_0 j \eta_0 b. \end{aligned} \quad (25)$$

To obtain some idea of the meaning of this quantity, consider the difference between the velocities of the field lines anchored in the surfaces, $z = \pm b$ and $R = a$, of D through which flux passes in and out. Since the velocities $\mathbf{w}_{in/out}$ must match the plasma velocity on the relevant boundary of D , they are given by

$$\mathbf{w}_{in/out} = -\nabla\Phi_{in/out} \times \mathbf{B}/B^2. \quad (26)$$

Assuming $B_0 > 0$, we can now identify the surface through which flux enters D as $z = b$, and the surface through which flux leaves it as $R = a$, namely,

$$\mathbf{w}_{in} = -\nabla\Phi_{z=b} \times \mathbf{B}/B^2, \quad \mathbf{w}_{out} = -\nabla\Phi_{R=a} \times \mathbf{B}/B^2. \quad (27)$$

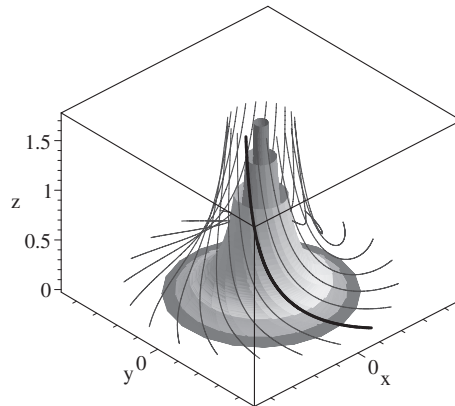


FIGURE 6 Flux surfaces of constant radius (for given z), within which field lines periodically exactly reconnect with themselves. For example, the highlighted (black) field line will split in the rotational flow, with the top ‘half’ remaining fixed, while the bottom ‘half’ reconnects with each of the grey field lines until eventually being reconnected again into the configuration shown after performing a rotation of 2π radians.

Now, $\Phi = \Phi_0$ on $z = b$, and hence $\nabla\Phi_{z=b} = \mathbf{0}$ and $\mathbf{w}_{in} = \mathbf{0}$, so field lines passing in through the top of D remain fixed and stationary there. Due to the rotational nature of \mathbf{v} , \mathbf{w}_{out} is also rotational, leading to a rotational mismatching between \mathbf{w}_{in} and \mathbf{w}_{out} . The value of F , given by Eq. (25), provides an idea of the maximum difference between the rate of rotation of the inward flux bundle and outward flux bundle, or the maximum rate of relative slippage (see Hornig and Priest, 2003, for a further pedagogic example). From Fig. 4b it can be seen that the outward bundle of field lines rotates approximately like a solid body close to the spine, with the rotation falling off to zero at the edge of the flux envelope.

As mentioned above, $\Delta\mathbf{w} = \mathbf{w}_{out} - \mathbf{w}_{in}$, the rate of slippage between the inward and outward bundles of field lines, is purely rotational, so that it has a θ -component only. Thus field lines are continuously reconnected in shells of constant radius (for a given value of z) only. These shells have the same three-dimensional shape as, and are concentric with, our flux envelope, see Fig. 6. An initial field line which splits into two will be periodically exactly reconnected with itself, every time the half embedded in $R = a$ performs a full rotation of 2π radians. Note, however, that this period is different for each shell, since it is not a rigid rotation. For this reason, if we consider a flux tube within the envelope with a finite radial extent, there will be no periodic return to the initial state.

It is important to note the implications the rotational slippage has for helicity production. If we imagine that the small flux tube within our flux envelope is closed somewhere far from D , then we can see that the relative rotation of the two ends of the tube would act to twist up the tube and thus act as a source of self-helicity with respect to an initially untwisted tube.

5 COMPOSITE SOLUTIONS

As discussed in Section 3, we may impose any ideal flow upon the solution described in the previous section, as shown in Eqs. (20) and (21). We would like to choose an

ideal flow which shows the global effect of the local rotational slippage behaviour by transporting magnetic flux into and out of the local flux envelope. For this reason, we choose to impose a stagnation-type ideal flow. Stagnation flows are physically relevant flows to choose as they may perform the localisation of the quantities contained in the non-ideal term in Eq. (5) (Priest and Forbes, 2000; Hornig and Priest, 2003), and are common in reconnection solutions, such as Craig and Fabling (1996).

The stagnation flow is chosen in such a way as to satisfy Eq. (21) by imposing a suitable $\Phi_{id}(x_0, y_0)$ on the surface $z = z_0$, and then substituting the inverse of the field line equations (12) to obtain $\Phi_{id}(x, y, z)$. The equivalents of Eq. (16) and (17) can then be used to find \mathbf{E}_{id} and $\mathbf{v}_{id\perp}$, respectively. Again, for ease of analysis, we choose to set $(\mathbf{v}_{id\perp})_z = 0$, via Eq. (23), to obtain \mathbf{v}_{id} . We choose to take

$$\Phi_{id}(x_0, y_0) = \varphi_0 x_0 y_0, \quad (28)$$

where φ_0 is a constant. The resulting flow, \mathbf{v}_{id} , takes the form of a stagnation-point flow, with separatrices coincident with the x - and y -axes in the plane $z = z_0$. For $z \neq z_0$, the flow separatrices are rotated with respect to this configuration, due to the spiralling of the magnetic field lines.

The total flow, obtained by adding this ideal flow to the elementary solution, and given by $\mathbf{v} + \mathbf{v}_{id}$, has the same stagnation-type structure outside the enclosing flux envelope, but inside we have a superposition of X-type and O-type flows. Whichever of these flows dominates is dictated by the nature of Φ near the spine, $R=0$. If we consider all other parameters fixed, there is a critical value of φ_0 , namely $\varphi_0 = \varphi_{crit}$, at which the transition from O-type to X-type flow takes place. This can be determined by examining the total Φ at small R , which (in cartesian coordinates) takes the form

$$\Phi = \beta + (x^2 + y^2)\gamma + (x^2 - y^2)\delta + \lambda xy + \mathcal{O}(x^3, y^3), \quad (29)$$

where

$$\begin{aligned} \beta &= \frac{B_0 j \eta_0}{91b^{12}} z(-7z^{12} + 26z^6 b^6 - 91b^{12}), \\ \gamma &= \frac{9B_0 j \eta_0}{5a^2} z, \\ \delta &= \varphi_0 \left(\frac{z}{z_0}\right) \cos \alpha \sin \alpha, \\ \alpha &= \frac{j}{4} \ln \left(\frac{z}{z_0}\right), \\ \lambda &= \varphi_0 (\cos^2 \alpha - \sin^2 \alpha) \left(\frac{z}{z_0}\right). \end{aligned} \quad (30)$$

In a plane of constant z , Φ changes from a local maximum to a saddle point, and thus the flow changes from O-type to X-type, when

$$4\gamma^2 - 4\delta^2 - \lambda^2 = 0.$$

Substituting in the above expressions for γ , δ and λ and rearranging for φ_0 we find that

$$\varphi_{crit} = \frac{18B_0j\eta_0z_0}{5a^2}. \quad (31)$$

For $\varphi_0 > \varphi_{crit}$, the flow is of X-type at the spine axis, whereas for $\varphi_0 < \varphi_{crit}$ it is O-type. Note that φ_{crit} is independent of z , so the flow type is the same for all z for a given value of φ_0 .

5.1 The Case $\varphi_0 > \varphi_{crit}$

For $\varphi_0 > \varphi_{crit}$, the stagnation flow dominates the rotational flow of the elementary solution everywhere, and hence \mathbf{v} , \mathbf{w}_{in} and \mathbf{w}_{out} all have a basic X-type structure. In order to analyse the effect the reconnection process has on rearranging the flux, we consider the mismatching of the two flux velocities \mathbf{w}_{in} and \mathbf{w}_{out} . The flow lines of these velocities are coincident with the contours of constant Φ_{in} and Φ_{out} , respectively. For clarity we examine the mismatching of these contours, and hence the flux velocities, in the plane $z=b$, without loss of generality. The two sets of contours are shown in Fig. 7. Note that the flow \mathbf{w}_{in} is exactly the ideal plasma velocity, \mathbf{v}_{id} , since the associated elementary solution from the previous section is zero on $z=b$. Note also that in the plane $z=b$, the boundary of the flux envelope associated with the elementary solution coincides with the boundary of the diffusion region, at $R=a$. The superposition of the flow lines of \mathbf{w}_{in} and \mathbf{w}_{out} is shown in Fig. 8a, which may be understood as follows. Consider a magnetic field line in an inflow region outside the diffusion region, whose intersection with the chosen plane, $z=b$, lies on one of the sketched flow lines. Outside D , the two sets of flow lines coincide (with each other and with \mathbf{v}), and the field line moves ideally. Once the field line is transported into D , the flux velocities \mathbf{w}_{in} and \mathbf{w}_{out} are no longer the same, and so we may choose to follow either the field line anchored in the ideal region above D , which moves at \mathbf{w}_{in} , or follow the field line anchored in \mathbf{w}_{out} . Plotting both motions the field line seems to split, as shown by the splitting of the flow lines.

There are three distinct types of behaviour of the magnetic flux, which occur in different regions of the flows. These regions are separated by the separatrices of the \mathbf{w} -flows, as well as those flow lines which just touch (but do not enter) D , all of

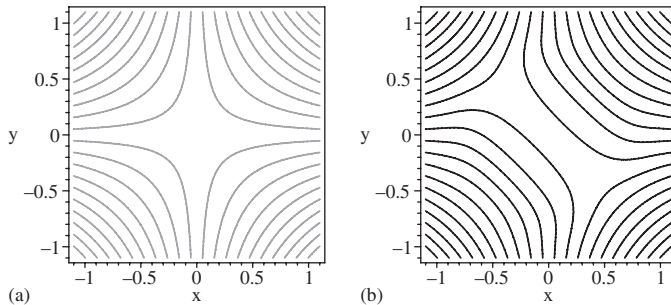


FIGURE 7 Flow lines in the plane $z=1$ of the field line velocities \mathbf{w}_{in} (a) and \mathbf{w}_{out} (b). The adopted parameter values are $B_0=1$, $a=1$, $b=1$, $\eta_0=1$, $j=1$, $\varphi_0=4 > \varphi_{crit}$.

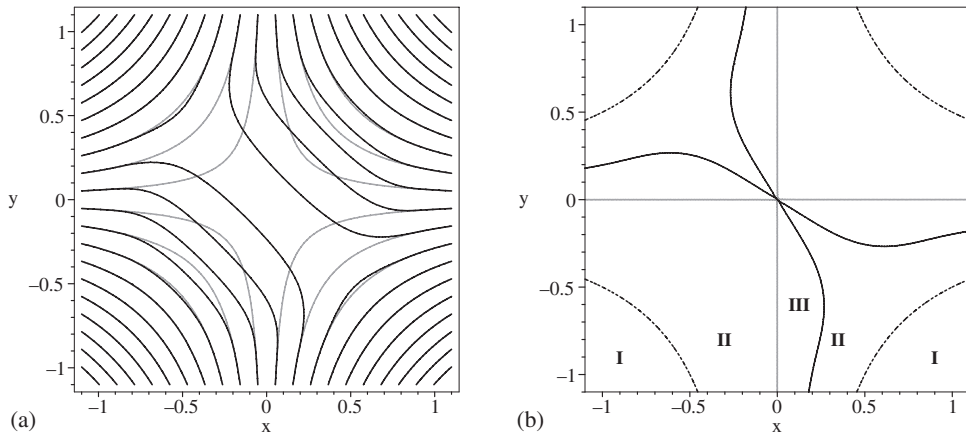


FIGURE 8 (a) The superposition of the two sets of flow lines shown in Fig. 7, highlighting the mismatching, and (b) the regions of different reconnective behaviour, distinguished by separatrices of w_{in} (grey) and w_{out} (black), as well as flow lines just touching the surface of D (dashed).

which are shown in Fig. 8b. Regions I show ideal behaviour everywhere. Here w_{in} and w_{out} coincide, and so field lines always remain connected and frozen to the plasma. In regions II, the flow lines split inside D , and so an initially unique field line splits, with each footpoint becoming differently connected. Notice, however, that although any two flow lines separate when they enter D , the same two flow lines always come back together when they leave D . We can therefore think of these regions as slippage regions, since, although in general the two ‘halves’ of the initial field line will take different times to pass through D , and will hence not rejoin upon leave D , they do move away from the reconnection region along the same flow line. Hence after both ‘halves’ of the field line have left D , their separation remains constant in time.

Regions III are quite different. Here again there is a splitting of flow lines, and thus field lines, at the edge of D . In contrast to regions II, however, the flow lines in this case never rejoin, and in fact head off in opposite directions. Hence after we leave D each footpoint of our initial field line is now connected to a field line from a topologically distinct region of magnetic flux. Regions III, then, can be thought of as more of a classical type of reconnection region, with the crucial characteristic being that initially joined field line footpoints continue to move away from each other for all time after leaving D . As φ_0 , and hence the strength of the ideal flow, is decreased, these classical reconnection regions grow in width, until we reach $\varphi_0 = \varphi_{crit}$.

5.2 The Case $\varphi_0 < \varphi_{crit}$

When $\varphi_0 < \varphi_{crit}$, the rotational flow dominates w_{out} near the spine, whereas w_{in} retains the X -type structure, as it still coincides with v_{id} . The two sets of flow lines and their superposition are shown in Figs. 9 and 10a. Again the different types of behaviour can be most clearly distinguished by studying the separatrices of these flows, which are shown in Fig. 10b. Regions I, II and III have essentially the same characteristic behaviours as before. Notice, however, that regions III where the classical flux separation occurs are now wider than when $\varphi_0 > \varphi_{crit}$ (if all other parameters are fixed). In addition we now have a region, marked IV in Fig. 10b, where the nature of the flux

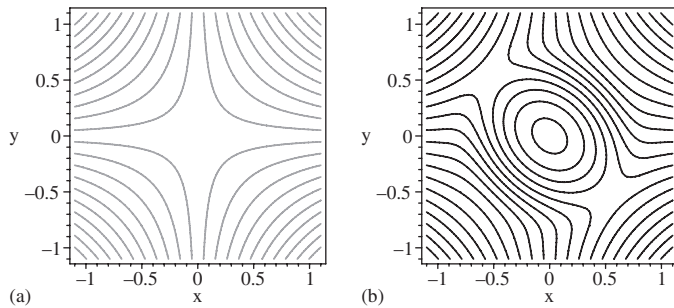


FIGURE 9 Flow lines in the plane $z=1$ of the field line velocities \mathbf{w}_{in} (a) and \mathbf{w}_{out} (b). The chosen parameters are $B_0=1$, $a=1$, $b=1$, $\eta_0=1$, $j=1$, $\varphi_0=1 < \varphi_{crit}$.

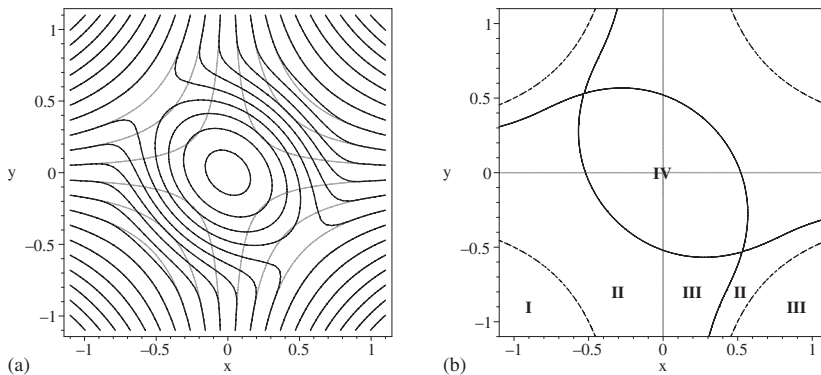


FIGURE 10 (a) The superposition of the two sets of flow lines shown in Fig. 9, highlighting the mismatching, and (b) regions of different reconnection behaviour, distinguished by separatrices of \mathbf{w}_{in} (grey) and \mathbf{w}_{out} (black), as well as flow lines just touching the surface of D (dashed).

reconnection is different again. In this region the flow lines of \mathbf{w}_{out} are closed, and so following a field line anchored in this flow, we find that it simply rotates round and round, never leaving the region or the local flux envelope. So we have a continuously rotating flux bundle moving at \mathbf{w}_{out} , which reconnects with a succession of different field lines, which are swept into and then out of the reconnection region at \mathbf{w}_{in} .

Note that the reconnection rate for both of the composite solutions described in this section is exactly the same as that given in Eq. (25) for the elementary solution, since $\Phi_{id} = 0$ when $R=0$, and so the calculation is unaffected. This reconnection rate now, however, summarises the sum of many different effects.

Lastly, note that the above analysis would follow through in exactly the same way had we chosen the option initially of integrating Φ from $R = R_0$. The only difference would be that flow lines of \mathbf{w}_{in} would become flow lines of \mathbf{w}_{out} and vice-versa.

5.3 Reconnection of Flux Tubes

To visualise the effect the mismatching of the field line velocities has on the reconnection of flux tubes, we now describe two examples. In each case, field lines are integrated from four arbitrary cross-sections chosen symmetrically about the spine such that initially we have two unique flux tubes on opposite sides of the diffusion region. The

cross-sections are chosen so that they never pass into the diffusion region, and hence we can identify a set of field lines which remains frozen into these cross-sections for all time, defining our flux tubes. The resulting motion of the flux tubes is plotted, although we stop the field line integration at a chosen point to see more clearly what is happening.

When the flux tube cross-sections are chosen to lie in region II, the resulting flux tube behaviour is a slippage, as described in Section 5.1, and shown in Fig. 11. We see that the flux tubes slip apart as they enter D , but the two sections of each initial flux tube leave the vicinity of the reconnection process in the same direction. The degree of slippage depends on the initial positions of the cross-sections, and the size of φ_0 .

The evolution of flux tubes whose cross-sections lie in regions III is shown in Fig. 12. Now the two sections of each flux tube flip around the spine in opposite directions after splitting. They then leave the diffusion region in opposite directions, as described in Section 5.1. Notice, however, that the four flux tubes formed during the splitting process never rejoin cross-wise to form two unique flux tubes again as they do in two-dimensional reconnection. They may share a few common field lines, although this need not necessarily be the case, depending on exactly where in region III the initial cross-sections are chosen.

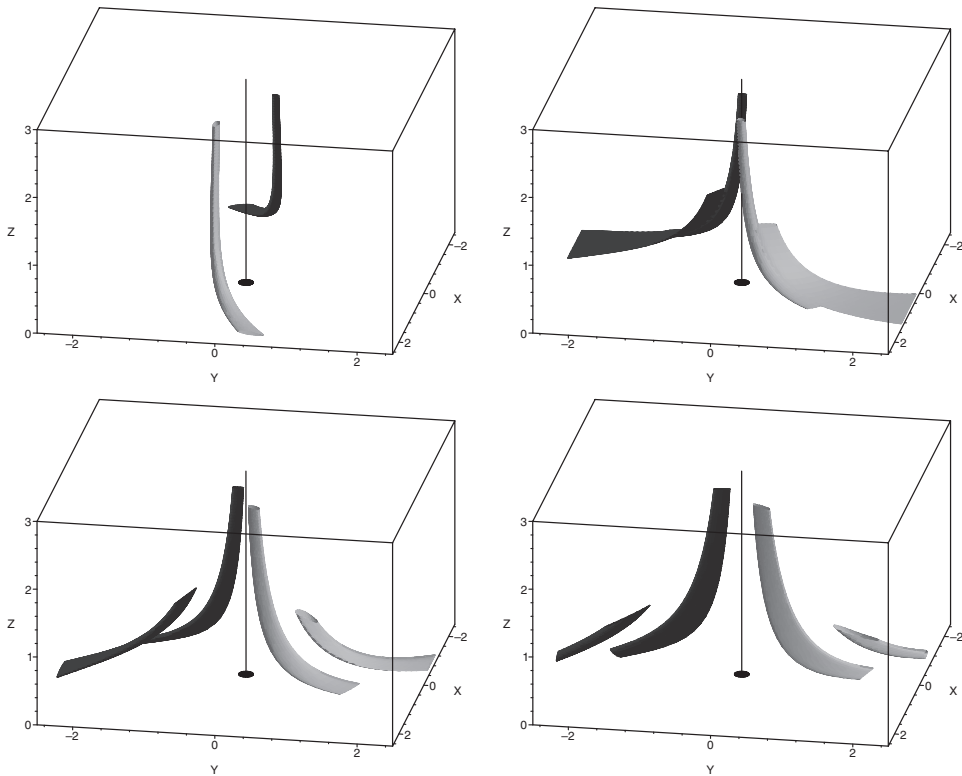


FIGURE 11 Evolution of a pair of flux tubes integrated from cross-sections lying in region II of the w -flows. As they enter the diffusion region each tube splits into two parts, which 'slip' apart, but on leaving D they move off in the same direction.

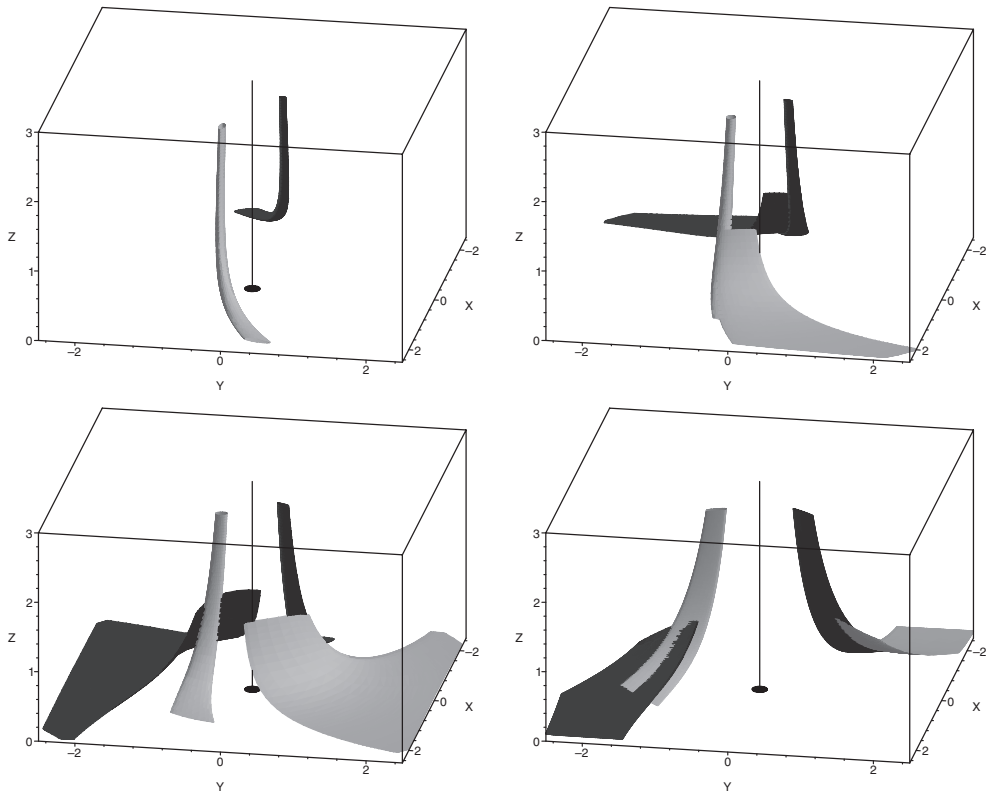


FIGURE 12 Evolution of a pair of flux tubes integrated from cross-sections lying in region III of the w -flows. As the tubes enter the diffusion region they split, with the two parts of each of the initial two tubes flipping around the spine in opposite directions. Notice in the final frame that after leaving D the four new tubes do not rejoin to form two unique tubes.

6 EXISTENCE OF PERFECTLY RECONNECTING FLUX TUBES AND TIME DEPENDENCE

We now ask whether it is possible to choose a pair of initial flux tubes which will perfectly rejoin after reconnection, such that we have two unique tubes before reconnection and two unique cross-wise connected tubes after reconnection. We have seen in the previous section that this is not generally the case, but perhaps with the right choice of initial cross-sections we can achieve this situation. In two dimensions, things are relatively straightforward. If we choose to pick out one field line, in an inflow region of v outside D , then it is always possible to find a corresponding field line, by simple symmetry through the X -point, with which it will perfectly reconnect. That is to say, if we label the two footpoints of field line 1 g_1 and h_1 , and of field line 2 g_2 and h_2 , then, if the field lines are chosen such that after reconnection g_1 is connected to g_2 , then h_1 will always be connected to h_2 (see Fig. 13a). So in two-dimensions there is a simple one-to-one reconnection of field lines, and hence flux tubes. In three dimensions this is not generally the case (Priest *et al.*, 2003), i.e., if g_1 becomes connected to g_2 after reconnection then h_1 will *not* be connected to h_2 (see Fig. 13b). In this sense there is

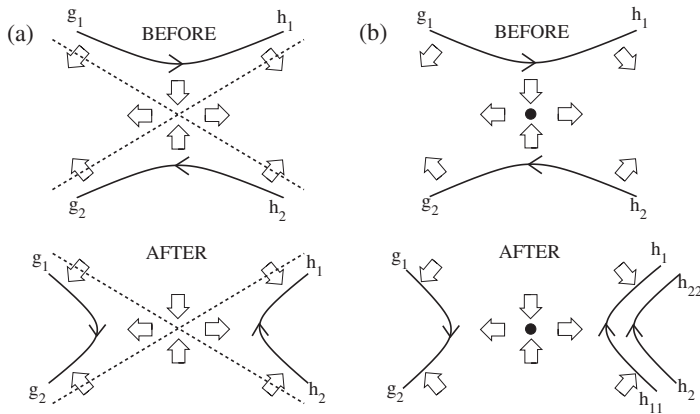


FIGURE 13 (a) The one-to-one reconnection of field lines in 2D. (b) Schematic picture of reconnection of field lines in 3D, for example top view of reconnection in region III of the composite solution of Section 5.

no one-to-one reconnection of field lines, so a given field line has no unique counterpart with which it becomes uniquely rejoined.

Nevertheless, if we can find two finite sets of field lines which reconnect with each other then we may still have perfect, or one-to-one, reconnection of these particular flux tubes. An iteration procedure for finding sets of field lines on either side of D which reconnect with each other is described in Hornig and Priest (2003). The procedure involves sequentially tracking field lines as they reconnect, moving in the flows \mathbf{w}_{in} and \mathbf{w}_{out} . In fact, in the stationary case it turns out that the sets of field lines which reconnect with each other lie in surfaces (see Fig. 14a), and so there are no perfectly reconnecting flux tubes.

We find that, if a simple time-dependence is introduced into η , as in Eq. (32), then perfectly reconnecting flux tubes can be found, as follows. Let

$$\eta = f(t)\eta_0 \begin{cases} [(R/a)^6 - 1]^2 [(z/b)^6 - 1]^2, & R < a, \quad z^2 < b^2, \\ 0, & \text{otherwise,} \end{cases} \quad (32)$$

where $f(t)$ is some arbitrary function of time only, and is thus effectively just a multiplicative constant in the calculation of Φ and \mathbf{E} described in Section 3. Hence $\nabla \times \mathbf{E}$ is still zero, and no extra magnetic field is induced. This time-dependence, then, shows up in Φ , \mathbf{E} , \mathbf{v} and thus \mathbf{w}_{in} and \mathbf{w}_{out} . By the same argument, a time-dependence could also be added to the ideal flow.

We will consider here the case where the ideal flow is still steady, and the diffusive process is localised in time via

$$f(t) = \exp(-t^2/T^2), \quad (33)$$

where T is a constant which controls the time-scale of the localisation. This time-dependence has little qualitative effect on the results described in the previous section, other than to localise the effect of the reconnection process in time.

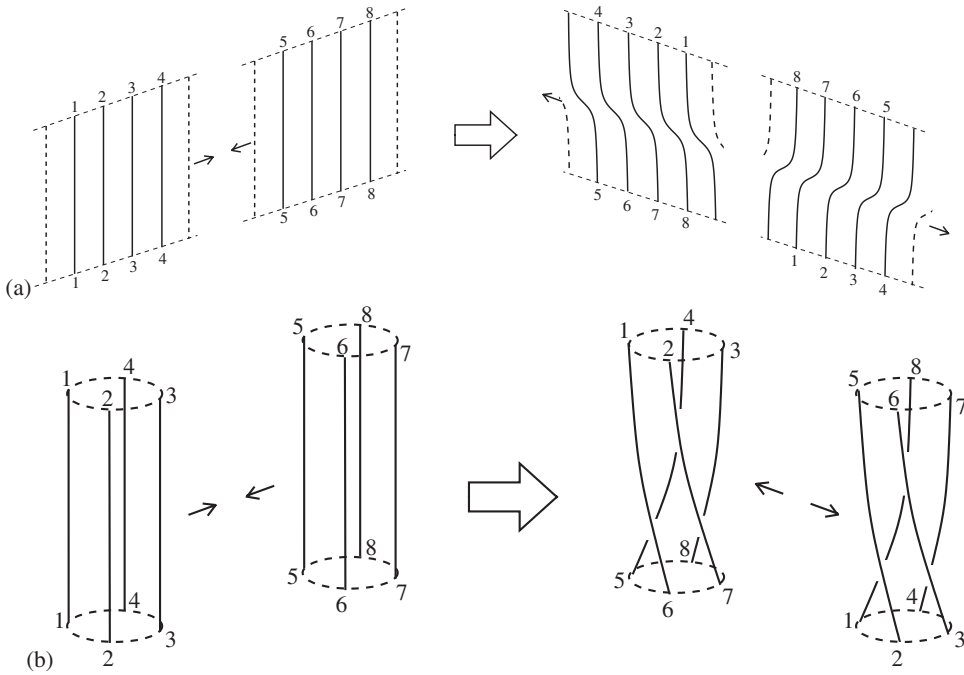


FIGURE 14 Schematic picture of reconnection of magnetic field lines in (a) a stationary state and (b) a time-dependent state, where there is one-to-one reconnection of flux tubes but not field lines.

In order to ensure numerical stability of the iteration process, we choose to add to the elementary solution a slightly different ideal solution to that described in the previous section. For the ideal potential, we choose

$$\varphi_{id} = \varphi_0 x_0 y_0 \exp [-(x_0^2 + y_0^2)/4], \tag{34}$$

so that the ideal solution is approximately the same as before near the diffusion region, but now the ideal velocity falls off with radius far away from the reconnection region. The flow lines and separatrices of \mathbf{w}_{in} and \mathbf{w}_{out} associated with the new composite flow are shown in Fig. 15, at $t = 0$.

We find that the result of adding the time dependence is that the flux surfaces of the stationary case close up to form flux tubes, as shown in Fig. 14b. Note that although these flux tubes do perfectly reconnect, there is still no one-to-one reconnection of field lines. For example, in the left hand tube footpoint 1 is connected to footpoint 6 after reconnection, whereas in the right hand tube footpoint 1 is connected to footpoint 8. The mapping of the field lines in the reconnected flux tubes shows a rotation, with respect to a one-to-one correspondence. This signifies the production of twist, and hence a finite amount of self-helicity due to the rotation, consistent with the idea of the elementary solution as a helicity source as described in Section 4.

The result of carrying out the iteration procedure is that the field line footpoints that we obtain trace out closed curves, shown in Fig. 16. These curves represent the cross-sections of perfectly reconnecting flux tubes in planes of constant z . Precisely what

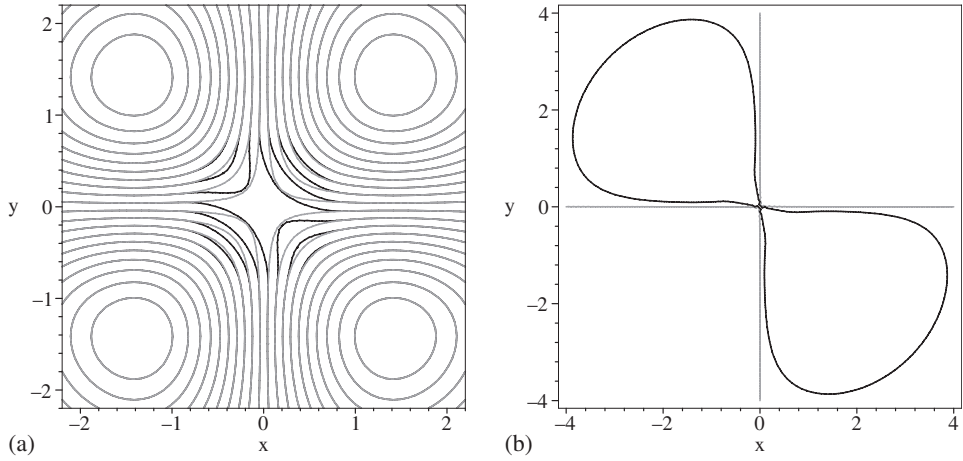


FIGURE 15 (a) Flow lines of \mathbf{w}_{in} (grey) and \mathbf{w}_{out} (black) for the modified time-dependent flow for $\varphi_0 > \varphi_{crit}$ and $t=0$ and (b) the separatrices of these flows.

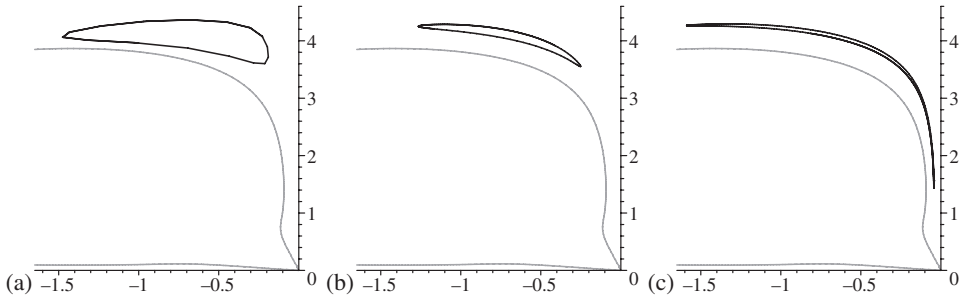


FIGURE 16 Perfectly reconnecting cross-sections in the time-dependent situation, in the plane $z=b$. For the parameters $a=1$, $b=1$, $B_0=1$, $\eta_0=1$, $j=1$, $\varphi_0=1$, and (a) $T=40$, (b) $T=200$ and (c) $T=800$. The grey lines are the separatrices of \mathbf{w}_{out} , while the separatrices of \mathbf{w}_{in} coincide with the x - and y -axes.

cross-sections are traced out depends on the starting point for the iteration procedure, with these cross-sections being concentric for fixed T . The effect of varying T , i.e. the localisation of the reconnection process in time, on the perfectly reconnecting flux tube cross-sections can be seen in Fig. 16. When the process is highly localised in time (T small) the cross-sections are fairly round, but as we increase T the cross-section becomes a thinner and thinner ellipse, whose major axis collapses towards a special time-symmetric flow line. When T is so large that we obtain a state which is numerically equivalent to the steady state, the iteration points (field lines) all lie along this flow line and we return again to a flux surface.

7 CONCLUSIONS

We have described here a steady solution of the kinematic resistive MHD equations, which exists in the vicinity of a spiral null point of the magnetic field, with a diffusion term localised around the null. Of course there are many other questions that will need

to be answered before a full understanding of these processes can be obtained, such as the role of Lorentz forces in producing the current sheet and driving the reconnection.

A rotational type of flux reconnection is found, similar to that described in Hornig and Priest (2003) for reconnection in the absence of a null point. The reconnection of magnetic flux takes the form of a rotational slippage within an envelope of flux enclosing the diffusion region. We note that this rotational form of slippage is independent of the size and shape of the diffusion region.

In order to study the effect of the process on the global magnetic field structure, an ideal flow was added which transports flux into and out of the local flux envelope. This results in different behaviours for field lines frozen into different regions of the ideal flow. In one region in particular, the rearrangement of the flux has some similar characteristics to two-dimensional reconnection, where the two parts of any field line (mapped from initially joined ends) separate, and the separation distance increases for all time. However, it is found that there is no simple one-to-one correspondence of reconnecting field lines after reconnection has occurred. As a result, there is also no splitting and one-to-one rejoining of flux tubes in the steady time-independent case. The result is that the re-ordering of flux by the reconnection process is much more complicated than at a familiar two-dimensional null point.

In the future, we plan to set up a numerical experiment for the full equations, including the equation of motion, and incorporating the invaluable insights that we have gained from this article. In particular, we shall calculate the flux motions \mathbf{w}_{in} and \mathbf{w}_{out} and will investigate whether the different types of kinematic reconnection that we have discovered here are realisable in the dynamic regime.

Acknowledgments

The authors would like to acknowledge financial support from the European Community Human Potential Program under Contract No. HPRN-CT-2000-00153, PLATON. G.H. would like to thank the VW-Foundation for financial support and D.I.P. is grateful to the Carnegie Trust for a PhD Scholarship.

References

- Antiochos, S.K., Karpen, J.T. and DeVore, C.R., "Coronal magnetic field relaxation by null-point reconnection", *Astrophys. J.* **575**, 578–584 (2002).
- Brown, D.S. and Priest, E.R., "The topological behaviour of 3D null points in the Sun's corona", *Astron. Astrophys.* **367**, 339–346 (2001).
- Bulanov, S.V. and Sakai, J., "Magnetic collapse in incompressible plasma flows", *J. Phys. Soc. Jpn.* **66**, 11, 3477–3483 (1997).
- Craig, I.J.D. and Fabling, R.B., "Exact Solutions for steady state, spine, and fan magnetic reconnection", *Astrophys. J.* **462**, 969–976 (1996).
- Fletcher, L., Metcalf, T.R., Alexander, D., Brown, D.S. and Ryder, L.A., "Evidence for the flare trigger site and three-dimensional reconnection in multiwavelength observations of a solar flare", *Astrophys. J.* **554**, 451–463 (2001).
- Hornig, G., "The geometry of reconnection", In: *An introduction to the geometry and topology of fluid flows* (Ed. R.L. Ricca), pp. 295–313, Kluwer, Dordrecht (2001).
- Hornig, G. and Priest, E.R., "Evolution of magnetic flux in an isolated reconnection process", *Phys. Plasmas* **10**, 2712–2721 (2003).
- Hornig, G. and Schindler, K., "Magnetic topology and the problem of its invariant definition", *Phys. Plasmas*, **3**, 781–792 (1996).
- Klapper, I., Rado, A. and Tabor, M., "A Lagrangian study of dynamics and singularity formation at magnetic null points in ideal three-dimensional magnetohydrodynamics", *Phys. Plasmas* **3**, 4281–4283 (1996).

- Lau, Y.-T. and Finn, J.M., "Three-dimensional kinematic reconnection in the presence of field nulls and closed field lines", *Astrophys. J.* **350**, 672–691 (1990).
- Longcope, D.W., "Topology and current ribbons: A model for current, reconnection and flaring in a complex, evolving corona", *Solar Phys.* **169**, 91–121 (1996).
- Longcope, D.W., Brown, D.S. and Priest, E.R., "On the distribution of magnetic null points above the solar photosphere", *Phys. Plasmas*, **10**, 3321–3334 (2003).
- Mellor, C. Titov, V.S. and Priest, E.R., "Linear collapse of spatially linear, three-dimensional, potential null points", *Geophys. Astrophys. Fluid Dynam.* **97**, 489–505 (2003).
- Parnell, C.E., Smith, J.M., Neukirch, T. and Priest, E.R., "The structure of three-dimensional magnetic neutral points", *Phys. Plasmas* **3**, 759–770 (1996).
- Parnell, C.E., Neukirch, T., Smith, J.M. and Priest, E.R., "Structure and collapse of three-dimensional magnetic neutral points", *Geophys. Astrophys. Fluid Dynam.* **84**, 245–271 (1997).
- Priest, E.R. and Forbes, T.G., *Magnetic reconnection: MHD theory and applications*, Cambridge University Press, Cambridge (2000).
- Priest, E.R. and Titov, V.S., "Magnetic reconnection at three-dimensional null points", *Phil. Trans. R. Soc. Lond. A*, **354**, 2951–2992 (1996).
- Priest, E.R., Heyvaerts, J.F. and Title, A.M., "A Flux-tube tectonics model for solar coronal heating driven by the magnetic carpet", *Astrophys. J.* **576**, 533–551 (2002).
- Priest, E.R., Hornig, G. and Pontin, D.I., "On the nature of three-dimensional magnetic reconnection", *J. Geophys. Res.* **108**, A7, SSH6-1 (2003).
- Schindler, K., Hesse, M. and Birn, J., "General magnetic reconnection, parallel electric fields, and helicity", *J. Geophys. Res.* **93**, A6, 5547–5557 (1988).